doi:10.1006/jmbi.2001.4739 available online at http://www.idealibrary.com on IDEAL® *J. Mol. Biol.* (2001) **309**, 1209–1218

JMB

Structural Assembly of the Active Site in an Aldo-keto Reductase by NADPH Cofactor

Gulsah Sanli and Michael Blaber*

Institute of Molecular Biophysics and Department of Chemistry, Florida State University, Tallahassee FL 32306-4380, USA

**Corresponding author*

A 1.9 Å resolution X-ray structure of the apo-form of *Corynebacterium* 2,5-diketo-D-gluconic acid reductase A (2,5-DKGR A), a member of the aldo-keto reductase superfamily, has been determined by molecular replacement using the NADPH-bound form of the same enzyme as the search model. 2,5-DKGR A catalyzes the NADPH-dependent stereo-specific reduction of 2,5-diketo-D-gluconate (2,5-DKG) to 2-keto-L-gulonate, a precursor in the industrial production of vitamin C. An atomic-resolution structure for the apo-form of the enzyme, in conjunction with our previously reported high-resolution X-ray structure for the holo-enzyme and holo/substrate model, allows a comparative analysis of structural changes that accompany cofactor binding. The results show that regions of the active site undergo coordinated conformational changes of up to 8 Å. These conformational changes result in the organization and structural rearrangement of residues associated with substrate binding and catalysis. Thus, NADPH functions not only to provide a hydride ion for catalytic reduction, but is also a critical structural component for formation of a catalytically competent form of DKGR A.

Keywords: aldo-keto reductase; NADPH; allostery; active site; catalysis

Introduction

Corynebacterium 2,5-diketo-D-gluconic acid reductase A (2,5-DKGR A) is a NADPH-dependent enzyme that catalyzes stereo-specific reduction of 2,5-diketo-D-gluconate (2,5-DKG) to 2-keto L-gulonate (2-KLG).[1] The enzyme is commercially important for the production of vitamin C because 2-KLG can be readily converted to L-ascorbate.[1–3] 2,5-DKGR A belongs to the aldo-keto reductase superfamily, and is also known as AKR5C in the newly proposed nomenclature.[4] Members of this family share the common $(\alpha/\beta)_8$-barrel (TIM barrel) structural motif and utilize NADP(H) as a cofactor.[5] The proposed catalytic mechanism[6] of DKGR A is similar to that of most of the aldo-keto reductase superfamily members,[7–9] constituting a two-step process in which an initial hydride ion transfer from cofactor to substrate occurs, followed by proton transfer from enzyme to the oxyanion intermediate.

Available biochemical data suggest that cofactor binding precedes substrate binding, and release of product precedes release of oxidized cofactor.[10–13] Furthermore, some members of this family exhibit biphasic substrate binding kinetics that may be related to structural changes upon cofactor and/or substrate binding.[13,14] Numerous X-ray structures have been determined for members of the aldo-keto reductase superfamily. However, the vast majority of these structures are enzyme/NAD(P)H or enzyme/NAD(P)H/inhibitor complexes. Almost nothing is understood about the structural changes that accompany cofactor binding.

We have previously reported a 2.1 Å X-ray structure of the DKGR A/NADPH complex,[15] as well as a molecular modeling study of substrate bound in the holo-enzyme.[16] In order to obtain a detailed description of coenzyme binding to 2,5-DKGR A, we carried out a crystallographic structural determination of the apo form. We report here the X-ray structure of apo 2,5-DKGR A at 1.9 Å resolution. A comparison of the apo and NADPH-bound structures of DKGR A indicates that a dramatic structural rearrangement occurs upon cofactor binding, with structural movements of up to 8 Å. Coordinated conformational changes

Abbreviations used: 2,5-DKGR A, 2,5-diketo-D-gluconate reductase A; NADP(H), nicotinamide adenine dinucleotide phosphate; NAD(H), nicotinamide adenine dinucelotide; 2,5-DKG, 2,5-diketo-D-gluconate; 2-KLG, 2-keto-L-gulonate; TIM, triosephosphate isomerase.

E-mail address of the corresponding author: blaber@sb.fsu.edu

0022-2836/01/051209–10 $35.00/0

are communicated over adjacent surface loops, and result in rearrangement and ordering of both catalytic residues and residues that comprise the substrate binding site. The results show that for DKGR A the role of the NADPH cofactor is not only to provide a hydride ion for reduction, but also to organize the active site into a catalytically competent structure.

Results

The crystallographic properties and refinement statistics of the apo DKGR A structure are listed in Table 1. Final model building and refinement resulted in excellent stereochemistry, with $R_{cryst} = 20.0\,\%$ ($R_{free} = 26.8\,\%$) for all data from 27.0 Å to 1.90 Å. Analysis of the Ramachandran plot distribution indicates that 91.4 % of the residue positions are located in the most favored regions, with no residues in disallowed regions. The Wilson temperature factor for the apo crystal is 16.1 Å^2 (Table 1), compared with 14.6 Å^2 for the $P2_1$ crystal form of the cofactor-bound form of DKGR A.[15] The average *B*-factor for main-chain and side-chain atoms in the refined apo structure are 17.3 Å^2 and 21.7 Å^2, respectively. These values are quite similar to those observed for the complex-bound form of DKGR A (15.9 Å^2 and 21.7 Å^2 for main-chain and side-chain atoms, respectively). A total of 1931 atoms and 271 solvent atoms (including two magnesium and two chloride ions) were included in the model.

The main-chain atoms of the apo DKGR A structure overlay those of the cofactor-bound structure[15] with an rms deviation of 1.1 Å (Figure 1). An analysis of the range and distribution of both C^α position and thermal factor shifts in comparison to the cofactor-bound structure indicates there are discrete regions exhibiting positional shifts, changes in thermal factors, or both, as a result of cofactor binding. These regions are delineated by residue positions 20-32, 45-55, 74-87, 106-116, 188-198, 229-241, 245-255 and 264-278 (Figure 1).

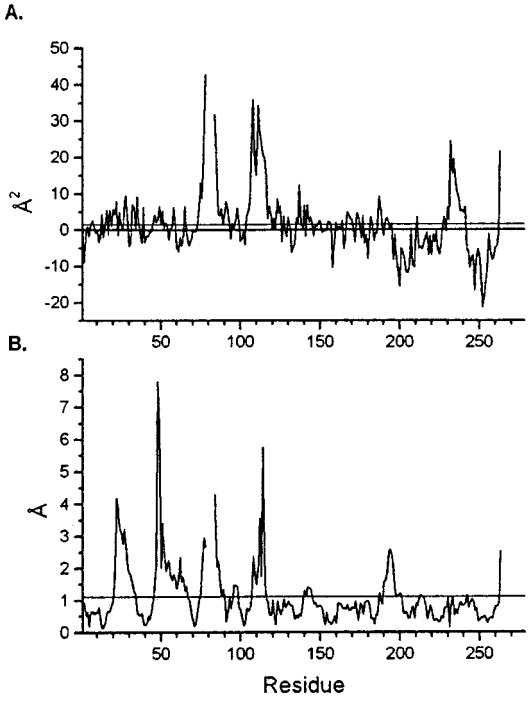

Figure 1. (Upper panel) ΔB-factor values for main-chain atoms of apo DKGRA in comparison to the cofactor-bound structure.[15] Postive values indicate that a residue in the apo structure has a higher refined thermal factor than the cofactor-bound structure. The horizontal line indicates the rms ΔB value of 1.5 Å^2. (Lower panel) ΔC^α values for apo DKGRA in comparison to the cofactor-bound structure. The horizontal line indicates the rms ΔC^α value of 1.1 Å.

Table 1. Crystal, data collection and refinement statistics

A. *Crystal data*	
Space group	$P2_12_12_1$
Cell constants (Å)	$a = 53.03$, $b = 53.94$, $c = 89.75$
Molecules/asymmetric unit	1
Matthews' constant (V_m) Å^3/Da	2.2
Maximum resolution (Å)	1.7
B. *Data collection and processing*	
Total/unique reflections	126,729/19,905
Completion (27.0-1.9 Å) (%)	94.5
Completion (1.94-1.90 Å) (%)	82.8
I/σ (overall)	15.6
I/σ (1.94-1.90 Å)	3.0
R_{merge} (%)	5.2
Wilson temperature factor (Å^2)	16.1
C. *Refinement*	
R_{cryst} (27.0-1.9 Å) (%)	20.0
R_{free} (27.0-1.9 Å) (%)	26.8
rms bond length deviation (Å)	0.007
rms bond angle deviation (deg.)	1.33
rms *B*-factor deviation (σ)[a]	2.1

[a] Library of Tronrud.[36]

Residues 20-32 comprise the carboxyl terminus of the β_1 central strand, the connecting loop to the α_1 helix, and the amino terminus region of the α_1 helix (Figure 2). This region is well defined in the electron density maps of both the apo and the cofactor-bound structures of DKGR A. The C^α thermal factors in this region exhibit similar values when comparing the apo and cofactor-bound structures; however, the polypeptide chain exhibits a positional shift of up to 4.2 Å (Figure 1). As an isolated structural segment, the main-chain atoms of region 20-32 from the apo form overlay the same region from the cofactor-bound form of DKGR A with an rms deviation of 1.0 Å. However, the main-chain atoms for residue positions 24-32 overlay with an rms deviation of only 0.28 Å. Thus, the main-chain positional shift observed for region 20-32 in the apo structure is composed of a rigid body motion for region 24-32 (in a direction away from the cofactor binding site) and a conformational change within region 20-23. Within

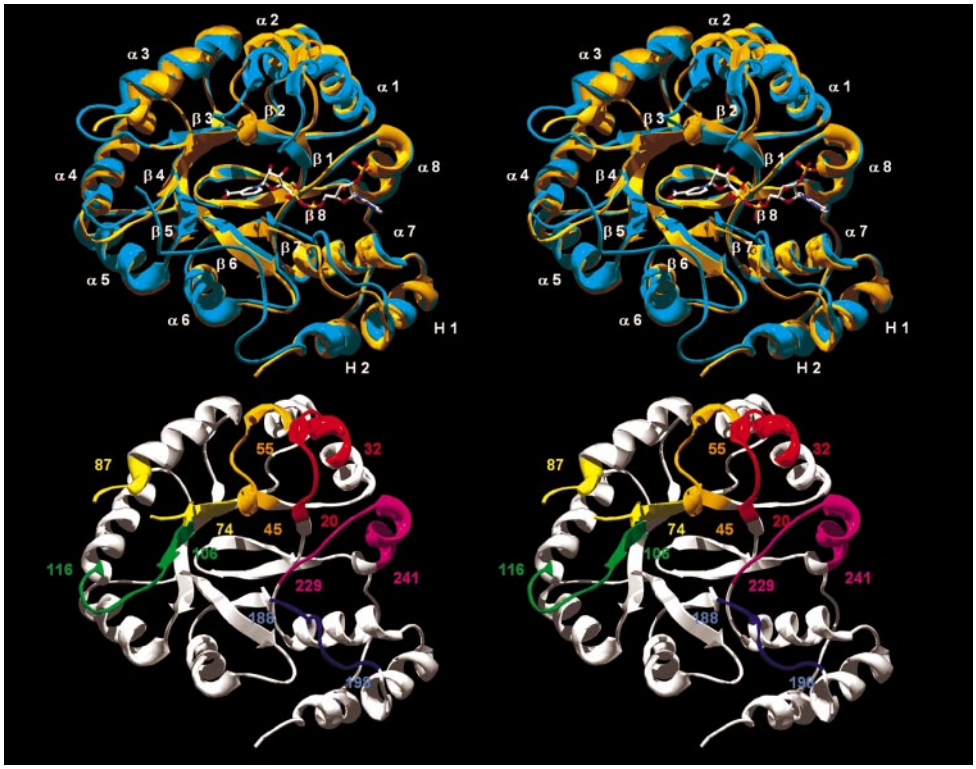

Figure 2. (Upper panel) Stereo view of a ribbon diagram of apo DKGR A (orange) overlaid with the NADPH bound structure (cyan).[15] Also shown is the location of the bound cofactor. The identification scheme for the secondary structure elements is also shown. (Lower panel) Stereo view of a ribbon diagram of apo DKGR A showing the location of regions of the structure that exhibit conformational and/or thermal factor changes upon cofactor binding. The residue positions that delineate these regions are also shown and are color coded as follows: residues 20-32 (red), residues 45-55 (orange), residues 74-87 (yellow), residues 106-116 (green), residues 188-198 (blue), residues 229-241 (magenta).

region 20-23, the main-chain amide of Phe22 is oriented away from the cofactor binding site in the apo structure (Figure 3). The polypeptide backbone of residues 20-24 in the cofactor-bound structure adopts an alternate conformation that rotates the peptide bond between residues 21 and 22 by approximately 100°. This orients in the main-chain amide of Phe22 towards the bound cofactor and permits a hydrogen bond interaction with the NO3 oxygen atom of the NADPH (Figure 3).

Residues 45-55 comprise the carboxyl terminus of the β_2 central strand, the connecting loop to the α_2 helix, and the amino terminus region of the α_2 helix (Figure 2). This region is well defined in the electron density maps of both the apo and the cofactor-bound structures of DKGR A. The C^{α} thermal factors in this region exhibit similar values when comparing the apo and cofactor-bound structures; however, the C^{α} atoms of the entire 45-55 region exhibit positional shifts of up to 7.8 Å when comparing the apo structure to the cofactor-bound structure (Figure 1). As an isolated structural segment, the main-chain atoms of region 45-55 from the apo form overlay the same region from the cofactor-bound form of DKGR A with an rms deviation of 2.9 Å and exhibit a significant conformational change (Figure 3). The O^{δ_1} atom of residue Asp45, at the start of region 45-55, forms a hydrogen bond with the NO2 oxygen atom of NADPH in the cofactor-bound structure. This residue is in a similar rotamer orientation in the apo structure and exhibits a relatively minor shift of 1.0 Å in response to cofactor binding. Residues 46-50 in the apo structure form a short stretch of α-helix at the carboxyl terminus of the β_2 central strand, prior to the connecting loop leading into the α_2 helix. However, in the cofactor-bound structure these residues form an extended main-chain conformation instead of an α-helix (Figure 3). This alternative conformation results in a positional shift of 7.8 Å for the C^{α} atom of Ala48. The conformational changes extend through residue Asn52, which upon cofactor binding is incorporated into the amino terminus of the α_2 helix extending it by one residue (Figure 3).

Residues 74-87 comprise the carboxyl terminus of the β_3 central strand, the connecting loop to the α_3 helix, and the amino terminus region of the α_3 helix (Figure 2). This region is poorly defined in the apo DKGR A structure, with essentially no electron density for residue positions 79-83. Flanking regions 74-78 and 84-87 exhibit C^{α} positional shifts of up to 4.3 Å, and increases in their *B*-factor values (Figure 1). The N^{δ_1} atom of Trp77 hydrogen

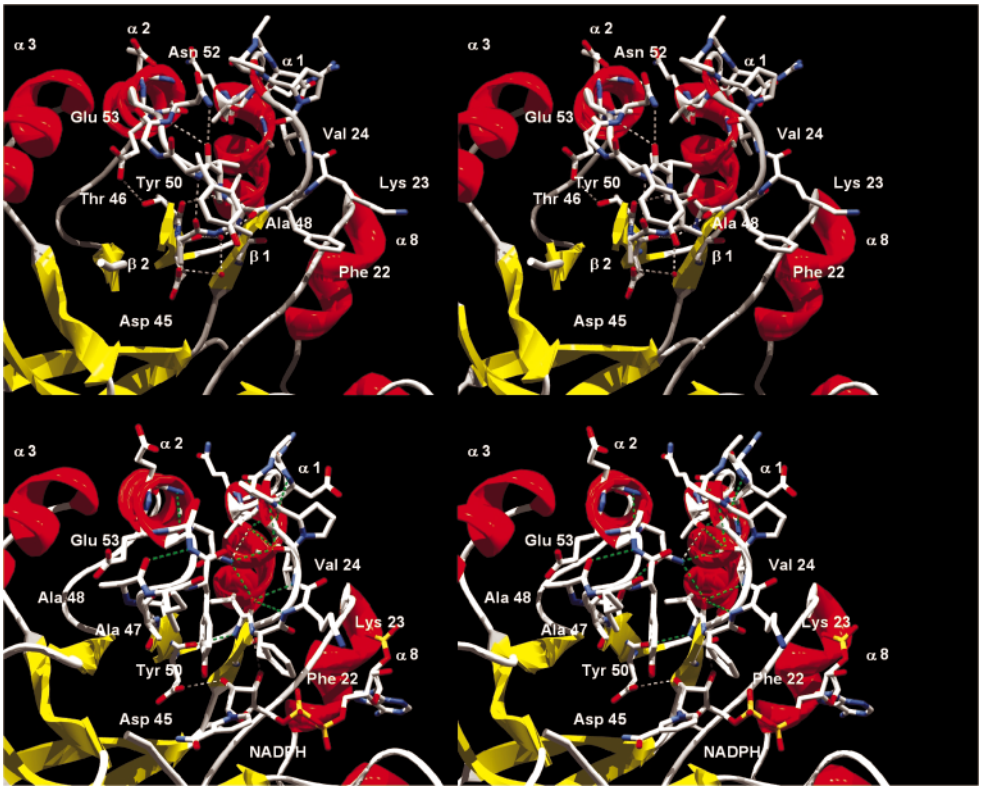

Figure 3. (Upper panel) Stereo view of regions 20-32 and 45-55 (wireframe) and a ribbon diagram of adjacent regions in the crystal structure of apo DKGR A. The ribbon diagram is colored by secondary structure as for Figure 1. Also shown are intra and inter-chain hydrogen bonds for these neighboring regions (the ribbon representation of the helix in region 47-48 is omitted for clarity) (Lower panel) Stereo view of the same regions from the NADPH/DKGR A complex structure.[15] Also shown is the NADPH cofactor and the intra and inter-chain hydrogen bonds between these regions and bound cofactor. The cooperative structural changes between these regions are apparent (see the text).

bonds with the main-chain carbonyl of Ala47 in the apo structure, also, the O^{γ_1} atom of Thr74 hydrogen bonds with the O^{γ_1} atom of Thr46 (Figure 4). The C^{α} atom of Trp77 is displaced 3.0 Å in response to cofactor binding, with the side-chain N^{ε}_{1} atom being displaced 7.2 Å. The side-chain of catalytic residue Lys75 has no defined electron density in the apo structure. In the cofactor-bound structure there is a well-defined hydrogen bond between the main-chain amide of His108 and the main-chain carbonyl of Leu76. Movement of both regions in the apo structure distorts the angle of this hydrogen bond by approximately 45°. Thus, this hydrogen bond is tenuous in the apo structure.

Residues 106-116 comprise the carboxyl terminus of the β_4 central strand, the connecting loop to the α_4 helix, and the amino terminus region of the α_4 helix (Figure 2). This region exhibits C^{α} positional shifts of up to 5.8 Å when comparing the apo and cofactor-bound structures, with the greatest positional deviation observed for the C^{α} of position 114 (Figure 1). This region also exhibits significant increases in thermal factors in the apo form (Figure 1). Contiguous electron density is present for residue positions 110-115 in the apo form, however, the electron density for residue positions 107-109 is discontinuous and poorly defined. No electron density is observed for the side-chain of catalytic residue His108 or adjacent Trp109 in the apo structure. As a segment, the main-chain atoms of this region from the apo form overlay the same region of the cofactor-bound form with an rms deviation of 1.9 Å, indicative of the conformational changes within this region (Figure 4).

Residues 188-198 comprise the carboxyl terminus of the β_7 central strand as well as the somewhat extended connecting loop leading to the H_1 helix (Figure 2). This region is well defined in the electron density maps of both the apo and the cofactor-bound structures of DKGR A. The C^{α} thermal factors in this region exhibit similar values when comparing the apo and cofactor-bound structures (Figure 1). However, the C^{α} atoms of this region exhibit positional shifts of up to 2.6 Å (Figure 1). As an isolated structural segment, the main-chain atoms of region 188-198 from the apo form overlay the same region from the cofactor-bound form with an rms deviation of 0.3 Å. Thus, the Cα positional shifts for this region can be described as a rigid body movement. Residues 188-198 move away from the cofactor binding site in the apo structure (Figure 2). Extensive interactions exist

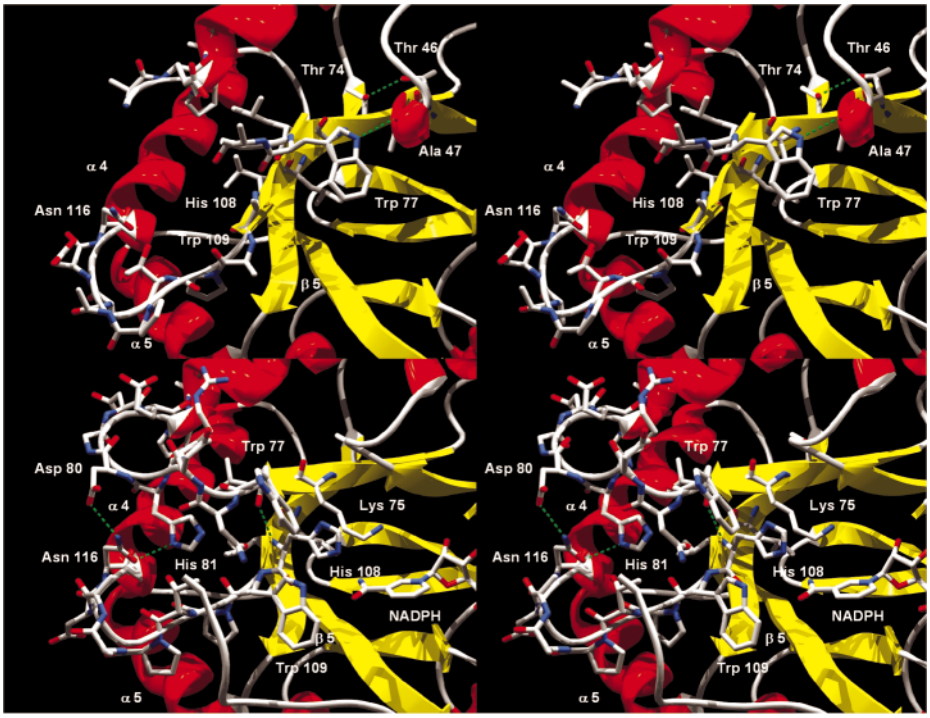

Figure 4. (Upper panel) Stereo view of regions 74-87 and 106-116 (wireframe) and a ribbon diagram of adjacent regions in the crystal structure of apo DKGR A. The ribbon diagram is colored by secondary structure as for Figure 1. Also shown in wireframe are residues Thr46 and Ala47. Hydrogen bonds between these groups and residues Thr74 and Trp77 are shown. (Lower panel) Stereo view of the same regions from the NADPH/DKGR A complex structure.[15] Intra-chain hydrogen bonds and key catalytic residues in these regions are indicated.

between bound cofactor and residue positions 187, 188, 190 and 192 in this region.[15] With the exception of Trp187, there are essentially only minor changes in atomic positions for the side-chains in this region between the apo and cofactor-bound forms. The side-chain of Trp187 forms an aromatic-stacking interaction with the cofactor nicotinamide ring in the cofactor-bound form of DKGRA. This side-chain adopts an alternative rotamer conformation in the apo form that orients the side-chain aromatic ring approximately 90° to that found in the cofactor-bound form.

Residues 229-241 comprise the carboxyl terminus of the β_8 central strand, the connecting loop to the α_8 helix, and the amino terminus region of the α_8 helix (Figure 2). This region exhibits minimal C^{α} positional shifts when comparing the apo structure to the cofactor-bound form of DKGR A, and main-chain atoms in this region overlay the associated atoms in the cofactor-bound structure with an rms deviation of 0.5 Å. However, the C^{α} atoms in this region display large increases in thermal factors in the apo form (Figure 1). The largest increase in thermal factors for C^{α} atoms in this region is observed for residue position Lys232, which increases from 10.3 $Å^2$ in the cofactor-bound form to 34.7 $Å^2$ in the apo structure, while its orientation in the structure is essentially unchanged. In the cofactor-bound structure hydrogen bonding interactions exist between the side-chains of residue positions 232, 233, and 238 and cofactor (particularly in the region of the NADPH terminal phosphate).[15] No electron density is observed for the side-chains of residue positions Ser233 and Arg238 in the apo structure.

Residues 245-255 are located on the amino-terminal face of the structure, in the loop connecting the α8 and H_2 helices (Figure 2). This region is on the opposite side from the cofactor-binding site as well as all structural changes observed in response to cofactor binding. Region 245-255 exhibits an unusual reduction in thermal factors in the apo structure compared to the cofactor-bound form. Residue Asp252 exhibits the largest decrease in *B*-factors ($\Delta B = -21$ $Å^2$) in the apo structure (Figure 1). Electron density in the solvent region adjacent to this side-chain exhibits a striking octahedral geometry. Modeling of water molecules in this density resulted in short contact distances (~2.1 Å) between the ''planetary'' and central solvent. Refined *B*-factors for the central solvent were typical of ordered water molecules in the structure. Due to the octahedral coordination, short contact distances with neighboring solvent, scattering similar to water, and interaction with an acidic side-chain, the central solvent at this position was modeled as a Mg ion.[17]

Residues 264-278 comprise the carboxyl-terminal loop region of the protein, beginning after the H_2 helix (Figure 2). No defined electron density is observed for the carboxyl-terminal region of apo DKGR A from residue 264 onward, whereas this

region is well defined in the cofactor-bound structure.[15]

Discussion

The structural changes between the apo and cofactor-bound forms of DKGR A are located exclusively on the carboxyl-terminal face (i.e. the cofactor-binding face) of the TIM barrel fold, with the exception of region 245-255. This region in the apo structure contains a bound magnesium ion (present in the crystallization mother liquor) that is not present in the crystal structure/mother liquor of the cofactor-bound form.[15] Binding of magnesium does not result in any structural perturbation other than a lowering of thermal factors in that region. The addition of magnesium chloride to DKGR A does not affect the kinetic properties of the enzyme,[6] but the reduced thermal factors suggests that magnesium ions may stabilize the structure. Thus, the thermal factor changes in region 245-255 appear related to the bound magnesium and not to cofactor binding. The majority of the structural changes related to cofactor binding occur in short, contiguous segments of the polypeptide chain delineated by the carboxyl-terminal region of a central β-strand, connecting loop, and amino-terminal region of an outer α-helix (Figure 2). Key regions undergoing conformational changes upon binding of cofactor include four adjacent strand-turn-helix regions of β_1/α_1 (residues 20-32), β_2/α_2 (residues 45-55), β_3/α_3 (residues 75-87), and β_4/α_4 (residues 106-115). Thus, the majority of the conformational changes are also localized to the amino-terminal half of the carboxyl-terminal face of the molecule (Figures 1 and 2).

Region 45-55 undergoes the most dramatic conformational change upon cofactor binding. Residues 46-50 form an α-helix in the apo structure, but exist as an extended region of the β_2 strand in the cofactor-bound structure (Figures 2 and 3). Amino acid residues in this region include Thr46, Ala47, Ala48, Ile49, and Tyr50. Alanine residues have the highest α-helix propensity of any amino acid.[18–20] Thus, in the absence of other interactions, an α-helical structure for region 46-50 follows from the intrinsic helical propensity. The electron density for this conformation in the apo form is unambigous.

Why does region 46-50 switch from an α-helix to an extended conformation in the presence of bound cofactor? Neighboring regions 75-87 and 106-115, which exhibit conformational changes, do not directly interact with cofactor. Thus, it appears that these regions are responding to structural changes in other parts of the molecule. The conformational change in region 46-50 is due to the interaction with cofactor and neighboring region 20-32. With regard to cofactor interaction, a hydrogen bond forms between the side-chain of residue Asp45 and the NO2 oxygen atom of the bound cofactor (Figure 3). This interaction is achieved with minimal structural rearrangement. The interaction with region 20-32, however, involves extensive and cooperative conformational changes. If region 21-24 rearranges to allow formation of the hydrogen bond between the main-chain amide of Phe22 and cofactor, the C^{α} atom of Phe22 and the side-chain C^{β} atom of Ala48 will have a close contact of 1.2 Å. It is this contact that precludes the structural rearrangement of region 21-24 without a corresponding rearrangement of region 46-50. The conformational change for region 46-50 not only eliminates this contact with region 21-24, but also allows additional hydrogen bonding interactions between these two regions. In the cofactor-bound structure the conformational change in region 45-55 also results in the amino-terminal of helix α_2 being initiated one residue earlier, by the incorporation of residue Asn52 in the helix. This reorients the side-chain of Asn52 towards region 20-32. The conformational change in region 21-24 not only positions the main-chain amide of residue 22 to hydrogen bond with cofactor, but also results in the main-chain carbonyl of residue 21 being juxtaposed to hydrogen bond with the (reoriented) side-chain of Asn52 (Figure 3).

What causes the structural ordering of region 74-87 upon cofactor binding? In the cofactor-bound structure there are no interactions between residues 74-87 and NADPH or residues 20-32. Thus, the ordering of region 74-87 is not due to direct interactions with these groups. If region 74-87 did not alter conformation in response to cofactor binding, then the structural changes in adjacent region 45-55 would result in close contacts of 1.0 Å between the side-chains of Ile49 and Trp77, and 2.1 Å between the side-chains of Tyr50 and Trp77. Furthermore, in the cofactor-bound structure atoms 45 O^{δ_1}, 46 O, and 50 OH form hydrogen bonds with the side-chain N^{ζ} atom of residue Lys75. This is made possible due to the conformational change in region 45-55 that rotates the main-chain carbonyl of residue Thr46 by approximately 180° relative to the cofactor-bound structure. Thus, the conformational changes observed in region 45-55 upon cofactor binding induce structural changes in region 74-87. Region 74-87 undergoes a disordered to ordered structure transition, including the catalytic residue Lys75.

As with region 74-87, there are no direct interactions between region 106-115 and bound cofactor. Therefore, the structural changes in region 106-115 in response to cofactor binding are communicated by other parts of the molecule. Region 74-87 interacts with region 106-115 through an extended group of direct, and solvent-mediated, hydrogen bonds in the cofactor-bound structure. The main-chain amide at position 109 interacts with atoms 76 O, 78 O^{δ_1} and 81 N^{ε_2} *via* solvent, additionally, the O^{δ_1} atom of residue 116 hydrogen bonds with the N^{δ_1} atom of residue 81. These interactions of region 74-87 with residues 109 and 116 do not exist in the apo form due to the disorder of region 74-87

(residue 78 is poorly defined, and residue 81 is not present in the apo model). Thus, the structural changes in region 74-87 result in structural changes within region 106-115.

No electron density is present for residues 264-278 in the apo structure. In the cofactor-bound form this region has interactions with the β_6-strand/turn region, the β_5-strand/turn region, regions 74-87 and 106-115, but no direct contact with NADPH (Figure 2). The interactions of region 264-278 within the β_6-strand/turn and the β_5-strand/turn regions are essentially unchanged between the apo and cofactor-bound structures. However, the main-chain carbonyl groups at positions 274 and 277 hydrogen bond through solvent with the main-chain amide at position 111. Structural changes in the region 106-116 of the apo structure reorient the main-chain amide of residue 111 by approximately 180° in relationship to the cofactor-bound structure. Thus, the solvent-mediated hydrogen bonding interactions between the main-chain carbonyl of positions 274 and 277 and the main-chain amide at position 111 are not possible in the apo structure. Likewise, the main-chain carbonyl groups at positions 277 and 278 hydrogen bond through solvent with the main-chain amide at position 113. Furthermore, the main-chain carbonyl at position 278 forms a direct hydrogen bond with the N^{δ_2} atom of side-chain Asn78. The hydrogen bonding interactions involving positions 277 and 278 with the residues in regions 74-87 and 106-115 are unique to the cofactor-bound structure and appear to be critical for ordering this segment. In this respect, the conformational changes induced in regions 74-87 and 106-115 by bound cofactor result in the ordered structure of the region 264-278 in the cofactor-bound form.

Comparisons of the apo and cofactor-bound forms of DKGR A show that binding of cofactor results in the structural movement, organization, and reorganization of specific regions of the molecule. Several of these regions contain residues involved in substrate binding and catalysis. Residue positions involved in catalysis include Tyr50, Lys75 and His108.[6–9,21] Tyr50 has been identified as the most likely donor for the protonation of the substrate oxyanion intermediate.[6,9,21,22] This residue is located within the segment of region 45-55 that switches from an α-helix to an extended conformation upon binding of cofactor (Figure 3). The side-chain and main-chain conformational changes for Tyr50 associated with this conformational switch result in a 5.9 Å movement of the critical side-chain OH group. Lys75 hydrogen bonds with Tyr50 OH in the cofactor-bound form (Figure 5), and may play a key role in lowering the pK_a value of this hydroxyl group to facilitate proton transfer.[21] While residue 75 is well defined in the electron density map of the cofactor-bound form, it is

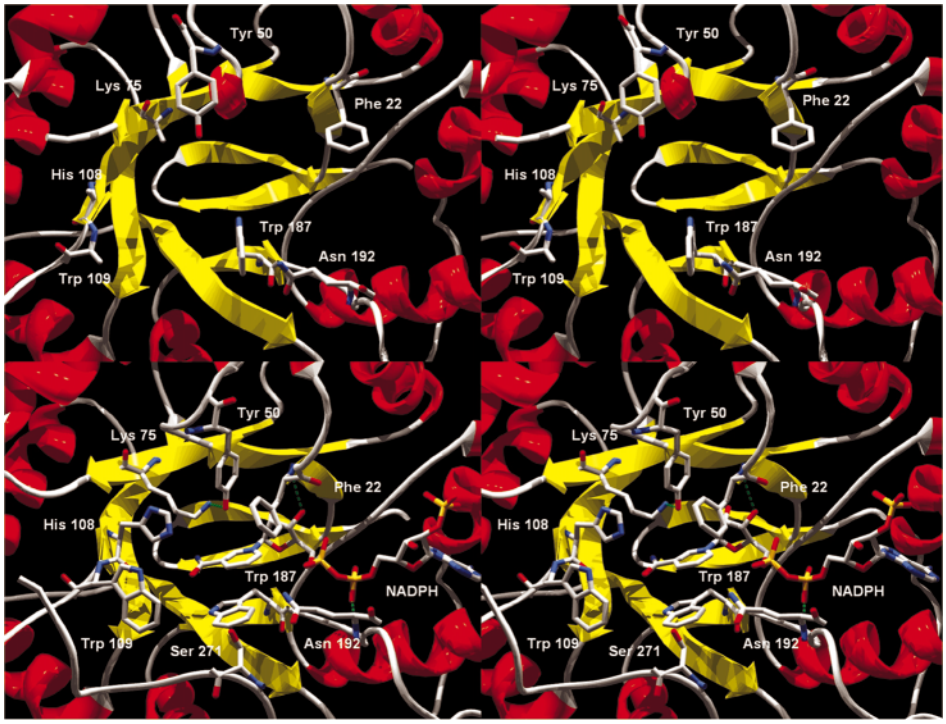

Figure 5. (Upper panel) Stereo view of active site region of apo DKGR A showing catalytic and active site pocket residues (wireframe) and a ribbon diagram of adjacent regions. The ribbon diagram is colored by secondary structure as for Figure 1. The side-chains of residues lysine 75, histidine 108 and tryptophan 109 are disordered and not present in the apo-structure (see the text). (Lower panel) Stereo view of the same region from the NADPH/DKGR A complex structure.[15] Also shown in this view is the location of the bound NADPH cofactor.

undefined in the apo structure. Therefore, binding of cofactor results in an ordered side-chain conformation for this catalytic residue. His108 is critical to catalysis, as demonstrated by mutagenesis experiments.[9,23] This residue has been suggested as another potential proton donor during catalysis, but most likely plays a critical role in substrate steering or electron delocalization during hydride ion transfer from cofactor.[21] Region 107-109 is poorly defined in the apo structure, and the lack of electron density for the side-chain of residues 108 and 109 indicates this region is disordered in the apo form. There is a 2.4 Å positional shift of the C^{α} atom of His108, in addition to well-defined side-chain electron density, in response to NADPH binding. Thus, cofactor binding results in the structural organization of all catalytically important residues to form an enzymatically competent active site (Figure 5).

The substrate binding pocket in the cofactor-bound structure is formed by residue positions Phe22, Tyr50, Lys75, His108, Trp109, Trp187, Gln192, Ser271, and NADPH.[15,16] Of this set of residue positions, the side-chains of Lys75, His108 and Trp109 are undefined in the apo form. Also, Ser271 is located within region 264-278 that is undefined in the apo form. Molecular modeling of substrate binding indicates that the N^{ε_1} atom of Trp109 hydrogen bonds with the substrate C4 hydroxyl group and that Phe22 participates in van der Waals contacts with substrate C6 carbon.[16] Phe22 exhibits a C^{α} positional shift of 4.2 Å, and a side-chain C^{ζ} positional shift of 6.1 Å in response to cofactor binding. Residue 50 has been described. The side-chain of Trp187 exhibits $\sim 100^{\circ}$ rotation, resulting in a 3.7 Å displacement of the side-chain N^{ε}_{1} atom. The side-chain rotamer of residue Gln192 is essentially unchanged in both the apo and NADPH-bound structures, with a C^{α} positional shift of 1.9 Å. Therefore, binding of cofactor results in an ordering or reorientation of almost the entire set of residues that define the substrate-binding pocket (Figure 5).

The set of residues comprising the cofactor-binding site include Phe22, Asp45, Ser139, Asn140, Gln161, Trp187, Gly188, Leu190, Gln192, Lys232, Ser233, Val234, Arg238, Glu241 and Asn242.[16] The majority of the side-chain and main-chain atoms of this group exhibit relatively small positional shifts in the apo *versus* cofactor-bound forms of DKGR A. The main-chain atoms of this group in the apo structure overlay with the equivalent atoms in the cofactor-bound structure with an rms deviation of 1.6 Å. However, if residue position Phe22 (describe above) is omitted from this set the rms deviation for the remaining set of residues is reduced to 0.8 Å. Atoms that interact with cofactor at positions Asp45, Asn140, Gln161, Lys232 (main-chain), Val234, Glu241 and Asn242 are similarly juxtaposed in apo *versus* cofactor-bound forms. The side-chains for residue positions Ser139, Trp187 and Lys232, which interact with cofactor, adopt alternative rotamer conformations in the apo *versus* cofactor-bound structures. The side-chains for positions Ser233 and Arg238, which interact with cofactor, are not visible in the apo structure. Therefore, the majority of residue positions that define the cofactor-binding site are appropriately positioned in the apo form to interact with cofactor.

The structural comparison of the apo and cofactor-bound forms of DKGR A demonstrate that NADPH cofactor provides not only a hydride ion for catalytic reduction of substrate, but is also a key structural component in organizing both the active site residues and the substrate binding pocket. The extensive structural changes observed here for DKGR A provide a possible structural interpretation for the kinetic evidence for a slow conformational change upon binding NADPH reported for pig muscle aldose reductase.[14] Reduction of substrate is concomitant with oxidation of NADPH to $NADP^{+}$. The presence of a cationic charge on the oxidized cofactor may destabilize interactions of cofactor with DKGR A, inducing a structural change back to the apo form. Thus, the conformational switch observed in the cofactor-bound *versus* apo form of DKGR A may provide a structural mechanism for the release of product and oxidized cofactor. Key to this structural change is the helix-coil transition of region 46-50, and the hypothesized role of alanine residues in this region. An alanine residue at position 47 in DKGR A is conserved at an equivalent position in 40 of the 42 members of the aldo-keto reductase superfamily.[7] Eleven members of this family with an alanine at position 47 also have alanine at position 48, and three members have alanine at positions 47, 48 and 49 (chalcone reductase from soy and alfalfa, and polyketide reductase from *Glycyrrhiza*). Thus, for these members of the superfamily, the region 46-50 in the apo forms may adopt a helical structure like DKGR A. However, the crystal structures of apo human and porcine aldehyde reductase (which contains two alanine residues at equivalent positions 47 and 48) show the extended rather than helical structure for this region.[24] However, a partially refined structure for the GCY1 protein from yeast (a member of the aldo-keto reductase family with alanine residues at positions 47 and 48) indicates a positional shift of approximately 4 Å for the active site tyrosine in the apo *versus* holo structures.[25] Therefore, perhaps only a subset of the aldo-keto reductase superfamily exhibits the conformational switch described here for DKGR A upon cofactor binding.

Materials and Methods

Crystallization of 2,5-DKGR A

Crystallization of *Corynebacterium* 2,5-DKGR A was accomplished using a synthetic gene construct and heterologous expression in *Escherichia coli*.[26] The expressed protein was purified using established procedures of sequential chromatography on Red A dye-affinity, anion exchange and size exclusion resins.[6,27,28] The purified

protein was concentrated to 13 mg/ml in 25 mM Tris-HCl (pH 7.5) for crystallization. Crystallization trials were set up using the hanging drop vapor diffusion method[29] and Hampton Crystal Screen I and II kit solutions (Hampton Research, Riverside, CA) at room temperature. Hanging drops contained a 1:1 mixture of protein and crystallization buffer (4 µl each) and vapor diffused against 1 ml reservoirs of crystallization buffer. Thin, plate-shaped crystals grew from 30 % (w/v) polyethylene glycol (PEG) 4000, 0.2 M $MgCl_2$ and 0.1 M Tris buffer (pH 8.5) within three to five days.

Data collection and processing

A single crystal (0.3 mm × 0.4 mm × 0.05 mm) was mounted on a cryo loop (Hampton Research, Laguna Niguel, CA) and X-ray diffraction data were collected at low temperature (103 K). Due to the presence of 30 % PEG 4000 in the crystallization buffer, no additional cryoprotectant was added. Data collection was performed using a Rigaku RU-H2R rotating anode X-ray source (40 kV, 100 mA, graphite monochromatic CuK_α radiation) equipped with an R-Axis IIc imaging plate system. The crystal diffracted to at least 1.7 Å resolution. Data were collected from this single crystal and processed using the DENZO software program. Indexing of the crystallographic data suggested an orthorhombic $P2_12_12_1$ unit cell (a different space group from the NADPH complex structure) with dimensions $a = 53.03$ Å, $b = 53.94$ Å and $c = 89.75$ Å. Based upon the molecular mass of approximately 29,000 Da,[28] one molecule in the asymmetric unit gave a V_m^{30} value of 2.2, suggesting that a single molecule represented the contents of the asymmetric unit.

Molecular replacement

The structure of apo 2,5-DKGR A was determined by the molecular replacement method using the refined 2.1 Å crystal structure of 2,5-DKGR A in complex with NADPH[15] as a search model (RCSB PDB accession number 1A80; space group $P2_1$). The NADPH cofactor and solvent were omitted from the search model. The rotation and translation function solutions were determined using the MRCHK software package.[31] A rotation function search, using data from 7.0-2.3 Å, resulted in a top solution with a signal of 5.8σ (next nearest peak 1.8σ). The correctly rotated model was used for a subsequent translation function search in space group $P2_12_12_1$. This search resulted in a top peak of 5.4σ, with the next highest peak at 4.3σ. This rotated and translated solution gave an initial value for R_{cryst} of 49.9 %, using all data from 27.0-3.5 Å. At this point it was apparent that close contacts existed between residues 208-210 and 22-25 in a symmetry-related molecule. The electron density appeared less well defined for region 208-210, and these residues were therefore deleted prior to rigid body refinement. Rigid body refinement of the model resulted in a slight improvement of R_{cryst} to 48.8 %. At this point 10 % of the data were separated for calculation of R_{free}.[32]

Refinement

The structure was refined using the TNT least-squares refinement package.[33,34] An initial round of individual atomic position refinement, using data from 27.0 Å-3.0 Å improved R_{cryst} to 37.2 % (R_{free} to 39.0 %) while maintaining excellent stereochemistry of the model. Inspection of the $2F_o - F_c$ electron density map for the entire structure indicated that significant rebuilding was required for regions 21-28, 78-84, 107-115 and 263-278. These regions of the model were therefore deleted prior to subsequent rounds of refinement. Manual model building was performed using $2F_o - F_c$, and $F_o - F_c$ omit maps and the molecular graphics program *O*.[35] Regions 21-28 and 107-115 could be built into regions of contiguous electron density, but no defined electron density existed for regions 79-83 and 263-278. Individual atomic coordinate refinement was performed in stages using data out to 2.5 Å resolution, at which point atomic thermal factors were simultaneously refined using a correlated thermal factor restraint library.[36] With the inclusion of all data to 1.9 Å, solvent molecules were added to the structure if they exhibited well-defined density in both the $2F_o - F_c$ and $F_o - F_c$ electron density maps, appropriate hydrogen bonding stereo-chemistry with neighboring groups, and refined thermal factors of 60 $Å^2$ or better.

Data Bank accession code

Model coordinates and structure factors have been deposited with the RCSB PDB (ID code 1HW6).

Acknowledgments

We thank Dr T Somasundaram for expert assistance during data collection. This work was supported by the American Heart Association (established investigator grant 0040235N) and the Florida State University Council on Research and Creativity.

References

1. Anderson, S., Marks, C. B., Lazarus, R., Miller, J., Stafford, K. & Seymour, J. *et al*. (1985). Production of 2-keto-L-gulonate, an intermediate in L-ascorbate synthesis, by a genetically modified *Erwinia herbicola*. *Science,* **230**, 144-149.
2. Sonoyama, T., Tani, H., Matsuda, K., Kageyama, B., Tanimoto, M. & Kobayashi, K., *et al*. (1982). Production of 2-keto-L-gulonic acid from D-glucose by two-stage fermentation. *Appl. Environ. Microbiol.* **43**, 1064-1069.
3. Reichstein, T. & Grussner, A. (1934). Eine ergiebige synthese der L-ascorbinsaure (C-Vitamin). *Helvetica Chim. Acta,* **17**, 311-328.
4. Jez, J. M., Flynn, T. G. & Penning, T. M. (1997). A new nomenclature for the aldo-keto reductase superfamily. *Biochem. Pharmacol.* **54**, 639-647.
5. You, K., Arnold, L. J., Allison, W. S. & Kaplan, N. O. (1978). Enzyme stereospecificities for nicotinamide nucleotides. *Trends Biochem. Sci.* **3**, 265-268.
6. Powers, D. P. (1996). PhD thesis, University of Medicine and Dentistry of New Jersey.
7. Jez, J. M., Bennett, M. J., Schlegel, B. P., Lewis, M. & Penning, T. M. (1997). Comparative anatomy of the aldo-keto reductase superfamily. *Biochem. J.* **326**, 625-636.
8. Wilson, D. K., Bohren, K. M., Gabbay, K. H. & Quiocho, F. A. (1992). An unlikely sugar substrate site in the 1.65 Å structure of the human aldose reductase holoenzyme implicated in diabetic complications. *Science,* **257**, 81-84.

9. Tarle, I., Borhani, D. W., Wilson, D. K., Quiocho, F. A. & Petrash, J. M. (1993). Probing the active site of human aldose reductase. Site directed mutagenesis of Asp43, Tyr48. and His110. *J. Biol. Chem.* **268**, 25687-25693.
10. Davidson, W. S. & Flynn, T. G. (1979). Kinetics and mechanism of action of aldehyde reductase from pig kidney. *Biochem. J.* **177**, 595-601.
11. Ryle, C. M. & Tipton, K. F. (1985). Kinetic studies with the low-K_m aldehyde reductase from ox brain. *Biochem. J.* **227**, 621-627.
12. Boghosian, R. A. & McGuinness, E. T. (1981). Pig brain aldose reductase: a kinetic study using the centrifugal fast analyzer. *Int. J. Biochem.* **13**, 909-914.
13. Grimshaw, C. E., Shahbaz, M. & Putney, C. G. (1990). Mechanistic basis for non-linear kinetics of aldehyde reduction catalyzed by aldose reductase. *Biochemistry,* **29**, 9947-9955.
14. Kubiseski, T. J., Hyndman, D. J., Morjana, N. A. & Flynn, T. G. (1992). Studies on pig muscle aldose reductase: kinetic mechanism and evidence for a slow conformational change upon coenzyme binding. *J. Biol. Chem.* **267**, 6510-6517.
15. Khurana, S., Powers, D. B., Anderson, S. & Blaber, M. (1998). Crystal structure of 2,5-diketo-D-gluconic acid reductase A complexed with NADPH at 2.1 Å resolution. *Proc. Natl Acad. Sci. USA,* **95**, 6768-6773.
16. Khurana, S., Sanli, G., Powers, D. B., Anderson, S. & Blaber, M. (2000). Molecular modeling of substrate binding in wild-type and mutant *Corynebacteria* 2,5-diketo-D-gluconate reductases. *Proteins: Struct. Funct. Genet.* **39**, 68-75.
17. Bock, C. W., Kaufman, A. & Glusker, J. P. (1994). Coordination of water to magnesium cations. *Inorg. Chem.* **33**, 419-427.
18. Lyu, P. C., Liff, M. I., Marky, L. A. & Kallenbach, N. R. (1990). Side-chain contributions to the stability of alpha-helical structures in peptides. *Science,* **250**, 669-673.
19. O'Neal, K. T. & DeGrado, W. F. (1990). A thermodynamic scale for the helix-forming tendencies of the commonly occurring amino acids. *Science,* **250**, 646-651.
20. Blaber, M., Zhang, X.-J., Lindstrom, J. D., Pepiot, S. D., Baase, W. A. & Matthews, B. W. (1994). Determination of α-helix propensity within the context of a folded protein, sites 44 and 131 in bacteriophage T4 lysozyme. *J. Mol. Biol.* **235**, 600-624.
21. Schlegel, B. P., Jez, J. M. & Penning, T. M. (1998). Mutagenesis of 3 alpha-hydroxysteroid dehydrogenase reveals a ''push-pull'' mechanism for proton transfer in aldo-keto reductases. *Biochemistry,* **37**, 3538-3548.
22. Varnai, P. & Warshel, A. (2000). Computer simulation studies of the catalytic mechanism of human aldose reductase. *J. Amer. Chem. Soc.* **122**, 3849-3860.
23. Bohren, K. M., Grimshaw, C. E., Lai, C.-J., Harrison, D. H., Ringe, D., Petsko, G. A. & Gabbay, K. H. (1994). Tyrosine-48 is the proton donor and histidine-110 directs substrate stereochemical selectivity in the reduction reaction of human aldose reductase: enzyme kinetics and crystal structure of the Y48H mutant enzyme. *Biochemistry,* **33**, 2021-2032.
24. Elkabbani, O., Green, N. C., Lin, G. D., Carson, M., Narayana, S. V. L. & Moore, K. M. *et al*. (1994). Structures of human and porcine aldehyde reductase - an enzyme implicated in diabetic complications. *Acta Crystallog. sect. D,* **50**, 859.
25. Hur, E. & Wilson, D. K. (2001). The crystal structure of the GCY1 protein from *S. cerevisiae* suggests a divergent aldo-keto reductase catalytic mechanism. *Chem. Biol. Interact.* **130-132**, 527-536.
26. Sanli, G., Blaber, S. I. & Blaber, M. (2001). Reduction of wobble-position GC bases in corynebacteria genes and enhancement of PCR and heterologous expression. *J. Mol. Microbiol. Biotechnol.* **3**, 123-126.
27. Miller, J. V., Estell, D. A. & Lazarus, R. A. (1987). Purification and characterization of 2,5-diketo-D-gluconate reductase from *Corynebacterium* Sp. *J. Biol. Chem.* **262**, 9016-9020.
28. Sonoyama, T. & Kobayashi, K. (1987). Purification and properties of two 2,5-diketo-D-gluconate reductases from a mutant strain derived from *Corynebacterium* sp. *J. Ferment. Technol.* **65**, 311-317.
29. Jancarik, J. & Kim, S.-H. (1991). Sparse matrix sampling: a screening method for crystallization of proteins. *J. Appl. Crystallog.* **24**, 409-411.
30. Matthews, B. W. (1968). Solvent content of protein crystals. *J. Mol. Biol.* **33**, 491-497.
31. Zhang, X.-J. & Matthews, B. W. (1994). Enhancement of the method of molecular replacement by incorporation of known structural information. *Acta Crystallog. sect. D,* **50**, 675-686.
32. Brunger, A. T. (1992). Free *R* value: a novel statistical quantity for assessing the accuracy of crystal structures. *Nature,* **355**, 472-475.
33. Tronrud, D. E. (1992). Conjugate-direction minimization: an improved method for the refinement of macromolecules. *Acta Crystallog. sect. A,* **48**, 912-916.
34. Tronrud, D. E., Ten Eyck, L. F. & Matthews, B. W. (1987). An efficient general-purpose least-squares refinement program for macromolecular structures. *Acta Crystallog. sect. A,* **43**, 489-501.
35. Jones, T. A., Zou, J. Y., Cowan, S. W. & Kjeldgaard, M. (1991). Improved methods for the building of protein models in electron density maps and the location of errors in these models. *Acta Crystallog. sect. A,* **47**, 110-119.
36. Tronrud, D. E. (1996). Knowledge-based *B*-factor restraints for the refinement of proteins. *J. Appl. Crystallog.* **29**, 100-104.

Edited by I. A. Wilson

(Received 15 February 2001; received in revised form 27 April 2001; accepted 1 May 2001)